Synthesis of single- and multi-wall carbon nanotubes over supported catalysts

A. Fonseca[1], **K. Hernadi**[1,2], **P. Piedigrosso**[1], **J.-F. Colomer**[1], **K. Mukhopadhyay**[1], **R. Doome**[1], **S. Lazarescu**[1], **L.P. Biro**[1,3], **Ph. Lambin**[1], **P.A. Thiry**[1], **D. Bernaerts**[4], **J. B.Nagy**[1]

[1] Institute for Studies in Interface Science, Facultés Universitaires Notre-Dame de la Paix, Rue de Bruxelles 61, B-5000 Namur, Belgium
[2] Applied Chemistry Department, Jozsef Attila University, H-6720 Szeged, Rerrich B. ter 1, Hungary
[3] KFKI-Research Institute for Materials Science, H-1525 Budapest, P.O. Box 49, Hungary
[4] EMAT, University of Antwerp (RUCA), Groenenborgerlaan 171, B-2020 Antwerp, Belgium

Abstract. Catalytic synthesis and some characterization of multi- and single-wall carbon nanotubes are presented. Supported transition-metal catalysts were prepared by different methods and were tested in the production of nanotubes by decomposition of hydrocarbons at 700 °C, using a fixed-bed flow reactor.

The quantities of deposited carbon were measured and the quality of the nanotubes was characterized by means of transmission electron microscopy and scanning tunneling microscopy. The inner and outer diameters of the nanotubes were also measured and the diameter distribution histograms were established. The multi-wall straight and coiled nanotubes were found to be quite regular with an average inner (outer) diameter of 4–7 nm (15–25 nm) and with lengths up to 50 μm. The walls contain concentric cylindrical graphene sheets separated by the graphitic interlayer distance. The single-wall nanotubes were found as bundles of hundreds of aligned straight 1-nm-diameter nanotubes with lengths up to 1-μm.

The influence of various parameters such as the method of catalyst preparation, the nature and the pore size of the support, the nature of the metal, the quantity of catalyst active particles, and the reaction conditions on the nanotubes formation were studied. The numbers and dimensions of the catalyst active particles dispersed on the support were found to be of importance in regulating the shape of the produced nanotubes. Following these results, a model of growth mechanism was suggested for the nanotubes obtained by this method.

The recent discovery of fullerenes [1], fullerenic onions [2], and hollow turbostratic carbon tubes of nanometer diameter [3] opened a new chapter in carbon chemistry. Because of their calculated chemical and physical properties [4–7], speculations about the possible applications of carbon nanotubes have been reported [8–10]. For the synthesis of carbon nanotubes several methods have been reported. The arc-discharge method developed for C_{60} synthesis supplied a very surprising result, namely the growth of fullerene tubes on the car-
bon cathode [3, 11–14]. Other nanotube synthesis methods were also used such as plasma decomposition of hydrocarbons [15, 16] and co-evaporating a catalyst during a carbon arc-discharge [17–21]. Single-wall nanotubes could be produced by the catalytic method evaporating cobalt or iron in the system. Recently, another catalytic process involving decomposition of hydrocarbons over supported catalysts and working under relatively mild conditions has been reported for carbon nanotube production [22, 23]. Compared with other synthesis methods, the selectivity of this process to carbon nanotubes is significantly higher [24]. The advantages of the latter method increase if applying zeolites as catalyst supports [25]. Single- and multi-shell nanotubes of regular dimensions are produced by catalytic decomposition of hydrocarbons over Co/Y-zeolite catalysts.

1 Experimental

Different silica- and zeolite-supported transition-metal (Co, Cu, and Fe) catalysts have been prepared and tested for the decomposition of hydrocarbons – mainly acetylene – at 700 °C.

1.1 Catalyst preparation

Method A: pH-controlled ion-adsorption precipitation on silica gel. As a first step, 1.056 g of cobalt salt [$Co(H_3C-CO_2)_2$ · $4H_2O$, Riedel-de Haën] were dissolved in 60 ml of distilled water for each sample.

Six as-made cobalt solutions were set to different pH values (for checking the pH, Merck "Neutralit" pH indicator strips were used). The pH of the original Co acetate solution was 7.0 and acetic acid or ammonia solution was used to set the pH of the solutions to 4, 5, 6, 8, and 9.

After this, 2.0 g of silica ("silicagel-20, -40, -60 or -90", Merck, particle size 15–40 μm) was added to each sample and they were left to stand and stirred occasionally. After two days the pH of the samples was shifted to the lower values.

For example, the pH = 9 (pH = 8) value changed to pH = 7 (pH = 6.5). Then, the samples were filtered in a Büchner funnel, washed with 2×50 ml of distilled water, and dried at 100 °C. This procedure was followed by calcination in air at 450 °C for 4.5 h.

In method A' a portion (0.4 g) of each sample from method A was hydrogenated in H_2/N_2 (H_2 flow, 35 ml/min, N_2 flow, 75 ml/min) at 650 °C for 8 h. One of the samples was treated in air (instead of hydrogen) under the same conditions (method A'').

Method B: Porous impregnation of zeolites, clays and silica gels. For the catalyst preparation, the impregnation method using a silica (silicagel-60, Merck), clay, or zeolite (NaY, Union Carbide; NaZSM-5, NESTE, Finland; NaA) support was applied. Co- or Fe acetate solution was used in the catalyst preparation procedure. Catalyst samples were calcined at 450 °C for 4.5 h. The final Co or Fe content of the impregnated samples was about 2.5 wt %.

1.2 Characterization of the catalyst samples

The cobalt content of the different fresh catalyst samples was determined by proton-induced X-ray emission (PIXE), using a Van de Graaf system (High Voltage Engineering N.V.), operating at 2.7-MeV proton beam.

Decomposition of acetylene was studied in a fixed-bed flow reactor (quartz tube of 14 mm in diameter in a Stanton Redcroft horizontal oven) at 700 ± 5 °C with a reaction time of 30 min. Each reaction was carried out using the same flow of acetylene (8 ml/min, Alphagas) and nitrogen (75 ml/min, Alphagas) and a catalyst amount of about 30 mg. The exact amounts of the initial catalyst and the carbon deposit formed during the reaction were determined by weighing and the reproducibility was within 10%. After decomposition of acetylene, the carbon yield was calculated for each reaction as follows:

$$\text{carbon yield}(\%) = 100(m_{\text{tot}} - m_{\text{cat}})/m_{\text{cat}}, \tag{1}$$

where m_{cat} is the initial amount of the catalyst (before reaction) and m_{tot} is the total weight of the sample after reaction.

The nature of the carbon deposit on the catalyst surface was characterized by transmission electron microscopy (TEM, Philips CM 20 and JEOL 200 CX). For sample preparation, the catalyst samples after reaction were glued on Rh−Cu grids. This method makes it possible to examine a representative sample of the product. It is therefore a good technique for judging the general quality of the sample. The gluing solution was made by suspending 0.5 m of tape (Scotch, 19 mm) in 100 ml of chloroform, followed by filtration.

For the STM analysis, samples were prepared by ultrasonication in toluene of the material (nanotubes and soot) resulting from the chemical removal of the catalyst by HF dissolution. As substrate, we used freshly cleaved highly orientated pyrolitic graphite (HOPG). Several droplets of nanotubes suspension in toluene were deposited on a freshly cleaved HOPG surface and the toluene was evaporated at room temperature. The samples were examined by STM under ambient conditions, using mechanically prepared Pt tips. Tunneling voltages in the range of 100–400 mV and tunneling currents in

the range of 0.2–1 nA were used. The horizontal and vertical calibration of the STM was checked against the HOPG substrate of the samples.

2 Results and discussion

The results on nanotube formation by catalytic decomposition of hydrocarbons are first described separately applying silica or zeolite support. Afterwards, the results from both of the sections are interpreted together, shedding some light on the growth mechanism of catalytically produced carbon nanotubes.

2.1 Applying silica support (preparation method A)

Both quantitative and qualitative analyses of carbon nanotube formation over different Co/silica catalysts are given. The carbon yields of acetylene decomposition over different Co/silica catalyst samples prepared by different methods are given in Table 1. In the same table, cobalt contents of the different catalyst samples determined by PIXE are also presented. These cobalt contents are lower than 0.1 wt % for samples of pH ≤ 6, around 1 wt % for samples of pH 7 to 8, and higher than 10 wt % for sample of pH = 9.

The general aspect of carbon nanotubes formed in the decomposition of acetylene at 700 °C over Co/silica is illustrated by the low-magnification TEM image in Fig. 1. Straight, coiled and helically wound carbon nanotubes can be observed in that figure. Nanotube adhesion, as well as a large mass of small nanotubes at the silica surface (black area) can also be observed. From the TEM image point of view, the main differences among the different samples are the silica surface coverage by nanotubes and the fraction of helical nanotubes.

2.1.1 Effect of pH *of catalyst preparation.* – Applying method A (Table 1): The highest activity was observed in the presence of catalyst prepared from the Co-acetate solution of pH = 8 both for the original and the hydrogenated samples (method A'). It is interesting to note that according to carbon yield data, there is no significant difference between catalysts prepared from solutions of pH = 7 and pH = 8. Otherwise, decreasing or increasing the pH of initial Co-acetate solutions results in a decreasing carbon yield. By making a comparison

Table 1. Carbon yields (% ± 10 rel. %) of acetylene decomposition at 700 °C over different Co/silica catalyst samples

Catalyst		Carbon yield /wt% ± 10 rel. %		
Initial pH	Final Co /wt%	Method A Calc. at 450 °C (air; 4.5 h)	Method A' Hydr. at 650 °C (H_2/N_2; 8 h)	Method A'' Calc. at 650 °C (air; 8 h)
4	< 0.01	7	15	—
5	< 0.01	9	23	—
6	0.04	51	45	—
7	0.82	71	76	—
8	1.74	74	83	—
9	11.64	47	65	58

between the original and the hydrogenated samples (Table 1), it can be concluded that the latter yield carbon in a somewhat higher amount.

Concerning the quality of the catalytically obtained carbon deposit (Fig. 1), a large amount of well-turbostratic carbon nanotubes covered only with a very small amount of amorphous carbon (Fig. 2) could be observed over the catalyst prepared from a Co-acetate solution of pH = 9 (method A). A definitely higher amount of helices is characteristic of the nanotubes produced over the pH = 9 samples.

The dimensions of the carbon nanotubes were quite regular, with outer diameters of 20–30 nm and inner diameters of 5–10 nm (Fig. 2). The length of the nanotubes was found to be of the order of 10 μm at the end of the reaction time of 30 min.
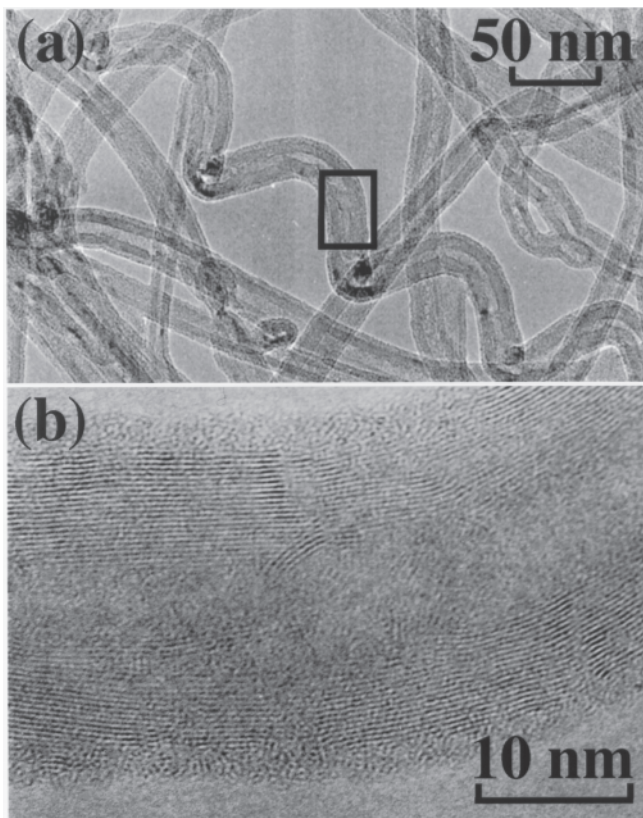
For the catalyst prepared from Co-acetate solution of pH = 8 (method A), the quality of the deposit was also very good, similar to the previous one. Over Co/silica (pH = 8; method A) we could also observe helices in relatively high percentage.

Whereas the activities of the catalysts prepared from solutions of pH = 7 and pH = 8 were about the same (Table 1), there was a significant difference between the qualities of carbon deposit formed on them. In the case of samples pH = 8 and pH = 9, every catalyst particle was covered by regular carbon nanotubes after the reaction (Fig. 1), but the composition of the product obtained over the catalyst pH = 7 was more heterogeneous. Much fewer particles were covered by well-turbostratic tubes, while the relative amount of irregular tubes and fibers increased considerably.

Observing the catalyst samples prepared from Co-acetate solution of lower pH, we saw that the surface was mostly covered by amorphous carbon and fibers. On Co/silica pH = 4 very few soot-like clusters could be observed by electron microscopy. The decreasing amount of carbon deposit at lower pH values (Table 1) can be related to the very low cobalt content of the catalysts prepared at acidic pH. In the absence of
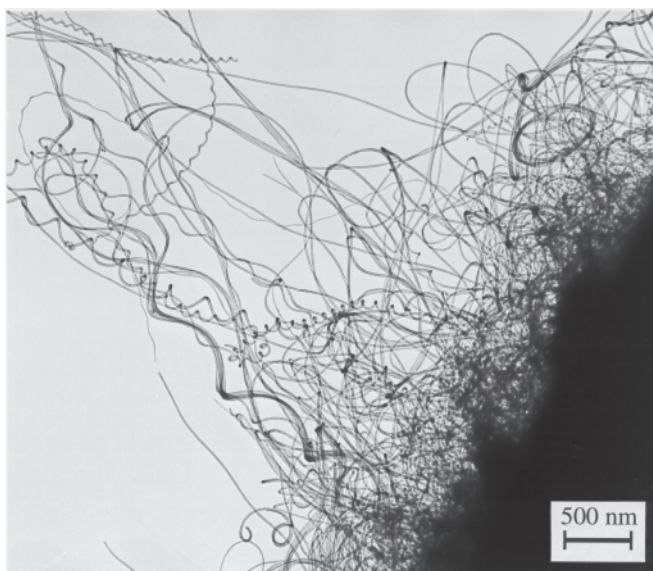
Fig. 2a,b. TEM images of carbon nanotubes formed in the decomposition of acetylene at 700 °C over Co/silica prepared by method A (pH = 9). **a** Medium magnification. **b** High resolution

metal particles, only the homolytic decomposition of carbon occurs, producing amorphous carbon and fibers.

– Applying method A' (Table 1): On the hydrogenated catalyst samples, a definite difference was observed in the quality of carbon deposit. Whereas over the original catalysts almost no amorphous carbon, soot, thick tubes, or fibers (over 50 nm in diameter) were found, the amount of these "by-products" was significantly higher on the hydrogenated samples. Many encapsulated cobalt particles are also observed on the hydrogenated catalysts [23].

– Applying method A'' (Table 1): One sample was pretreated in air at 650 °C for 8 h without hydrogenation (method A'' in Table 1). The behaviour of this catalyst is intermediate between that of the original and the hydrogenated samples, considering both carbon yield and the quality of carbon deposit. The quality of the tubes is almost as good as those obtained over Co/silica calcined at 450 °C but more amorphous carbon and thick tubes could be observed on the surface of the support.

– Generally: During the catalyst calcination at 450 °C thermal decomposition of Co acetate takes place and gives Co oxide. As a result of the applied calcination treatment, the first series of catalyst samples (method A in Table 1) should contain well-dispersed Co-oxide particles on the silica support, mainly in the inner pores. The hydrogenated series (method A' in Table 1) contain cobalt particles in a reduced form. Since the reactant acetylene is able to reduce the catalyst itself under the above-

Fig. 1. Low-magnification TEM image of carbon nanotubes formed in the decomposition of acetylene at 700 °C over Co/silica prepared by method A (pH = 9)

mentioned reaction conditions, reduction alone explains neither the higher catalytic activity leading to a higher carbon yield nor the appearance of amorphous carbon and thick fibers. According to our previous results [22], the diameter of the carbon nanotubes growing on a Co/silica particle depends mainly on the dispersion of the catalyst. During the hydrogenation treatment the catalyst was exposed to high temperature for a long time (compared to the average reaction time of 30 min). As a consequence cobalt particles had a chance to migrate from the inner pores to the outer surface and to assemble, reducing dispersion. These particles outside the pores can be reached by the reactant molecules more easily, which gives an explanation for the higher catalytic activity. At the same time increasing the particle size can result in the higher amount of amorphous carbon and thick tubes obtained over the hydrogenated catalyst samples. This shows that like long calcination at high temperature, hydrogenation also has a disadvantageous effect on the catalyst performance. Since acetylene is able to reduce Co-oxide particles to a required extent, more fortunate if the active sites are being formed in situ at the beginning of acetylene decomposition [30], it means that the most selective catalyst can be obtained during the induction period of the reaction. From electron microscope observations, it can be concluded that catalyst samples calcined at 450 °C for 4.5 h give better results in nanotube production than those that were calcined at 650 °C or reduced prior to acetylene reaction.

It is also interesting to point out that on certain bad samples – not selective in nanotube formation – it is possible to have a very high carbon yield (deposited in the silica pores) and still no carbon nanotubes at all when observing the samples by TEM. As it concerns mainly the samples pH = 4 and pH = 5, the cobalt concentrations of which are very low (< 0.01 wt %), it can be concluded that when there is not enough cobalt on the catalyst surface to form clusters big enough to have the *nanotube formation selectivity*, the low cobalt content of the catalyst will only contribute to a very high *carbon deposition activity*. The fact, that the carbon deposition is originated from the cobalt centers is in agreement with the absence of *carbon deposition activity* on pure silica. It behaves as if the *carbon deposition activity* depended mainly on the percentage of cobalt present on the catalyst after the set of pH and washing steps, while the basicity of the initial cobalt solution would control the *nanotube formation selectivity*.

2.1.2 Effect of transition-metal. Fe/silica prepared by the impregnation method (pH = 7) showed some inhomogeneity in the quality of carbon deposit (besides carbon nanotubes it contained some amorphous carbon and thick tubes having diameter larger than 50 nm also) and produced carbon yields of lower value, compared to Co/silica samples.

Using the ion-adsorption precipitation method (pH = 7) the properties of the Fe/silica catalysts were improved remarkably. Whereas the value of carbon yield increased above 100%, compared to Co/silica samples, the tubes became homogeneous in diameter and less amorphous carbon was observed. According to TEM observations, all catalyst particles are covered by carbon nanotubes of regular diameter.
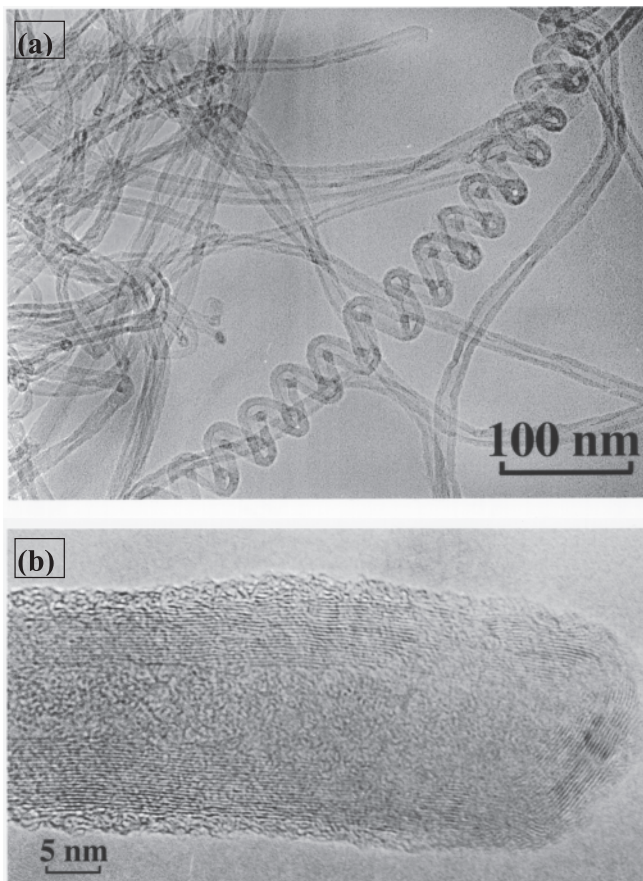
Fig. 3a,b. Carbon nanotubes formed in the decomposition of acetylene at 700 °C over Fe/silica catalyst, prepared by ion-adsorption precipitation at pH = 7. **a** Medium magnification. **b** High resolution

The average value of the outer diameter is approximately 10–20 nm and that of the inner diameter is 5–8 nm. Carbon nanotubes produced on Fe/silica (ion-adsorption precipitation) can be seen in Fig. 3.

As can be seen on high-resolution images (Fig. 3b), the structure of the nanotube inner wall is turbostratic for several layers – up to approximately one half of the tube wall – and that of the outer wall is mainly amorphous carbon. The tip of the nanotube is generally cupped by carbon material continuing the tube structure (Fig. 3b). According to TEM images, thicker tubes also exist and their inner wall structure is turbostratic too. The macroscopic appearance of this material can be described as follows. The product has a "spongy" texture and it is very fluffy and light, easy to charge electrostatically. The tubes stick to glass surfaces very strongly. After simply removing the catalyst bed, a fairly large amount (a few mg) of almost pure carbon nanotube could be collected by scraping the bottom of the quartz boat. It contains only a small amount of silica support and is free of amorphous carbon. The formation of spiral nanotubes could also be observed on Fe/silica catalysts as illustrated in Fig. 3a. As for the Co/silica catalysts, the formation of coiled nanotubes is clearly enhanced over the catalyst formed using a pH = 9 initial solution.

2.1.3 Effect of different hydrocarbons. Catalytic decomposition of acetylene, ethylene, propylene, and methane has

Table 2. Carbon yield as a function of reactant and reaction temperature over Fe/silica catalyst (ion-adsorption precipitation, pH = 7, 30 min reaction)

| Reactant	Carbon yield (wt% ± 10 rel. %)		
	at 700 °C	at 750 °C	at 800 °C
Acetylene	117	—	—
Ethylene	34	60	—
Propylene	33	39	—
Methane	0	0	±0

been checked at different reaction temperatures (Table 2). In the decomposition of ethylene and propylene at 700 °C, the carbon yield over Fe/silica (ion-adsorption precipitation, pH = 7) is much lower than in that of acetylene and the quality of carbon nanotubes was much poorer, so the formation of amorphous carbon and thick tubes became significant; the nanotubes were "crumbled", which showed that the organization of the wall was not good enough. Increasing the reaction temperature favoured the development of well-turbostratic structures and at the same time the amount of soot diminished to a great extent. For example, the carbon yield was found to be 60% at 750 °C in the reaction of ethylene (Table 2). Fe/silica was almost inactive in the decomposition of methane, even at 800 °C. At this reaction temperature, no carbon deposit could be weighed but a very small amount of amorphous soot has been observed by electron microscopy.

2.1.4 Purification of the MWNT (multi-wall-nanotubes). The MWNT produced over the different metal/silica catalysts generally contain some amorphous carbon and are linked to the silica support through the active metal particle. Purification then means separation of the MWNT from the silica, metal, and amorphous carbon.

– Separation of the MWNT from the metal/silica catalyst: By using a silica support, nitric acid treatment removed the transition-metal derivatives liberating the nanotubes from the catalyst surface. Afterwards, the ultrasound treatment was able to take some of the nanotubes into suspension. They were in the liquid phase after the heavy silica particles were decanted. However, the yield of nanotubes purified by this method was very low (approximately 1%) and – according to the X-ray diffractograms – the product still contained some small silica particles. Dissolving silica particles in HF seemed to be impossible, probably because of the carbon deposit covering the support. At this stage of the purification the yield was 1% for the Fe/silica catalyst and somewhat less for the Co/silica.

– Separation of the MWNT from the amorphous carbon: After the separation from the catalyst particles, the sample still contained a few percent of amorphous carbon. For removing this contamination, hydrogenation of the sample was carried out at 900 °C, for 4.5 h. According to a previous paper [23] this treatment is effective in the elimination of elemental carbon having irregular structure. Comparing reactivity of different carbon structures to hydrogen, it can be concluded that the reaction rate of amorphous carbon is significantly higher, which makes the method suitable for its separation from the graphitic forms. The yield of the hydrogenation treatment is about 25%.

2.2 Applying zeolite support (preparation method B)

Catalyst samples made by impregnation or by ion-exchange using Y zeolite have been tested in the decomposition of acetylene at 700 °C. Co/Y prepared by ion-exchange was found to be inactive in the formation of carbon nanotubes, whereas the samples made by impregnation showed high activity. A view of the general aspect of the nanotubes formed over metal/zeolite catalysts prepared by impregnation is given in Fig. 4a. The black part is the zeolite support and the carbon nanotubes can be seen linked to the zeolite surface by their bottom end. It is interesting to notice that no soot
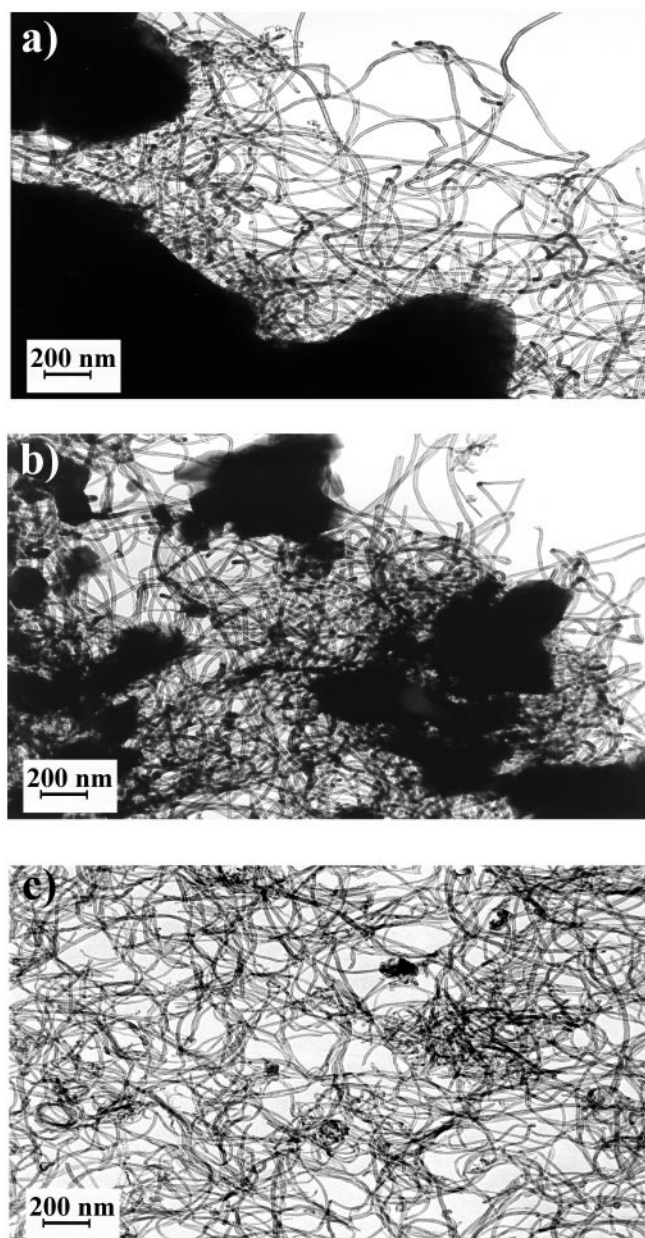
Fig. 4a–c. TEM images of straight, coiled, and helically wound carbon nanotubes formed in the catalytic decomposition of acetylene over Co/NaY catalyst at 700 °C. **a** As-made nanotubes linked to the Co/NaY catalyst. **b** Nanotubes and amorphous carbon recovered by filtration after dissolution of the catalyst in HF. **c** Pure nanotubes after removal of the amorphous carbon by oxidation in air

or mass of small nanotubes can be observed on the zeolite surface. This characteristic allows us to distinguish zeolite- from silica-supported catalysts covered with nanotubes, on the TEM images.

Co particles on the outer surface of the impregnated samples (in particular with Y zeolite) must be responsible for the activity and in this case zeolite can be by considered as a catalyst support. Since ion-exchanged CoY samples contain cobalt essentially in the inner pores, their inactivity in nanotube formation can be interpreted by considering that the ion-exchangeable cations have no effect on catalyst performance.

The relatively small volume of inner pores (compared to silica having pore diameters approximately ten times higher) provides the advantage that much less amorphous carbon is liberated from the inner pores during the purification procedure.

2.2.1 Effect of zeolite nature. Different zeolites such as HY, NaY, NaZSM-5, and NaA were used as catalyst support in carbon nanotube formation.

– Applying Fe/zeolite catalysts: No significant difference was found among the Fe/zeolite samples except that Fe/NaY catalyst gave better results than Fe/NaZSM-5 or Fe/NaA. Nor was there any real difference observed between NaY and HY since the nature of the ion-exchangeable cations has no effect on catalyst performance. Fe/NaA was found quite as active as Fe/NaY. Using Fe/NaZSM-5, not only was the activity decreased to about half of that of Fe/NaY, but also the turbostratic quality of the carbon deposit was poorer. It appears that the structure of the zeolite support may modify the effectiveness of the catalyst particles, leading to the differences observed between Fe/NaY, Fe/NaA and Fe/NaZSM-5 samples

– Applying Co/zeolite catalysts: No significant difference was found among the Co/zeolite samples, except that Co/NaY catalyst gave better results than Co/NaZSM-5 and Co/NaA.

2.2.2 Effect of transition-metal. According to TEM observations (Fig. 4) Co/NaY (prepared by the impregnation method) is able to produce regular nanotubes with average inner (outer) diameter of 2–9 (8–28) nm and with length at least $10 \, \mu m$. The activity of Fe/NaY is higher, so the amount of the weighed carbon deposit is bigger, but the quality of the nanotubes (turbostratic nature) is better over cobalt samples. The tubes from Fe/NaY seem to be more crumbled, just like those formed on Fe/silica (Fig. 3). No long and regular helices were found on the surface of Fe/NaY.

Other transition-metals such as palladium and platinum were also tested in the decomposition of acetylene. Neither Pd/NaY nor Pt/NaY showed selectivity in nanotube formation in our experimental conditions. Although Pt/NaY was found to be inactive, Pd/NaY could produce very few carbon nanotubes but the carbon deposit on its surface was composed mostly of irregular carbon nanofibers.

2.2.3 Separation of the nanotubes from the metal/zeolite catalyst. Separation of nanotubes and catalyst particles can be carried out by repeated dissolution of the zeolite support in hydrofluoric acid and filtering. The HF treatment (50 ml of 40% HF/g Co/NaY catalyst) was carried out on 2.803 g of sample (composed of 0.780 g carbon deposit and 2.023 g Co/NaY catalyst). Although some loss of nanotubes also occurs during filtration, because of the high cohesion between the nanotubes, filtration of the aggregated sample can be carried out with high efficacy. Comparing X-ray diffractograms of catalyst Co/Y, the sample after reaction, and the sample after HF treatment, it can be concluded that while in the first case the zeolite structure could be identified, in the last sample no Y zeolite was detected at all. On the TEM images of purified carbon nanotubes after the second HF treatment (Fig. 4b), carbon nanotubes and amorphous carbon (dark spots) released from the inner pores can be seen. It is also possible to see lots of regular nanotubes and some open tips. These open tips are liberated by the dissolution of the catalyst active particles in acidic media.

According to high-resolution electron microscope observations, the structure of the nanotubes are well-turbostratic and not much amorphous carbon was found on the surface [25]. Compared to silica support [24], zeolite dissolves more easily in hydrofluoric acid and contains much less amorphous carbon in the pores, which is released during the purification procedure. After three HF treatments, the yield of recovered carbon material is 100% of the total amount of carbon deposited on the catalyst.

2.2.4 Identification of the multi- and single-wall nanotubes by STM. In nanotube samples, only separated from the metal/zeolite catalyst by HF dissolution, individual tubes and bundles of tubes with 1-nm-diameter range have been found [31, 32]. A typical view of a large scale image of parallel nanotubes of about 1-nm diameter is shown in Fig. 5.

The 1-nm-diameter attribution to the nanotubes in the flat-lying bundle (Fig. 5a) was confirmed by many other plot profiles similar to the one displayed in Fig. 5b. These single-wall nanotubes were only observed by STM and not yet by TEM.

Considering the pore opening of Y zeolite (7.4 Å), only the formation of single-wall nanotubes (SWNT) with diameter smaller than that of C_{60} (10.0 Å) could be expected in the inner pores of the zeolite. But, at the places where half supercage is on the surface, a metal particle the dimension of which is regulated by the zeolite pore size (13.4 Å) can be deposited. The latter metal particle can catalyse the growth of half C_{60}. That half C_{60}, when extruded from the catalyst particle, can either grow to completion (forming C_{60}) or initiate the formation of a single-wall nanotube.

The formation of the bundles of single-wall nanotubes on the Co/NaY catalyst could be explained by the simultaneous growth of several nanotubes, out of the neighbouring zeolite open supercages at a zeolite crystallographic face. The centre-to-centre distance of the zeolite supercages being 12.35 Å, the most stable bundle of nanotubes to be produced on such a surface would be in the 12.35-Å-diameter range ((11,0) or (6,6) tubules for instance). In that case, the extra stabilization would be caused by intertubule distance being 3.4 Å (graphitic distance).

2.2.5 Identification of C_{60} – the smallest SWNT – by HPLC and MS. The soxhlet extraction of the crude nanotubes and Co/NaY catalyst with toluene for 48 h gives 0.13 wt % of fullerene C_{60} relative to the deposited carbon. The structure attribution to the C_{60} was done according to mass spectrometry,
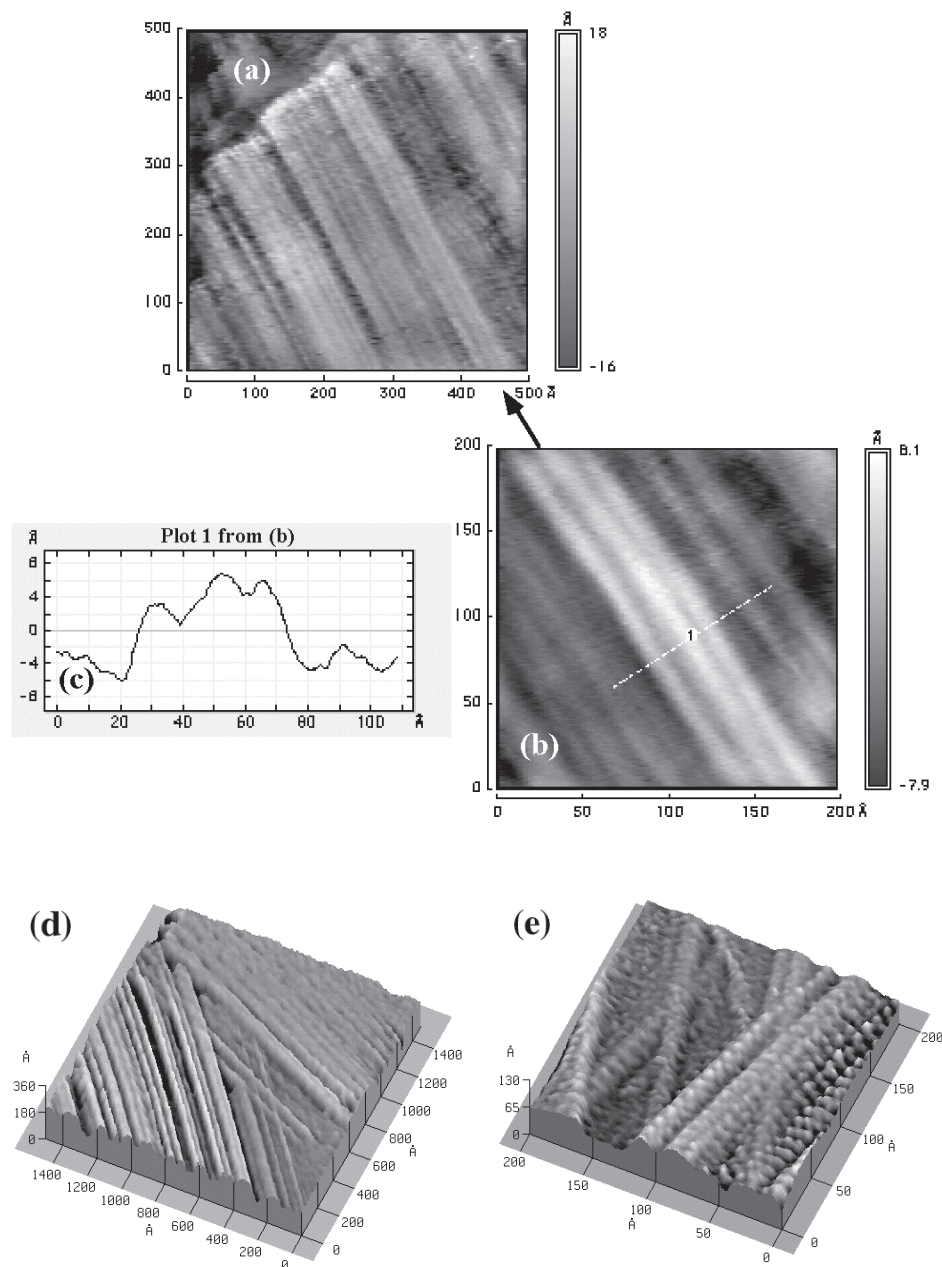
Fig. 5a–e. Constant-current STM images of a bundle of single-wall nanotubes separated from Co/NaY catalyst by HF dissolution of the catalyst. Both pictures were imaged with a mechanically cut Pt tip, in ambient conditions, at tunneling currents of 0.1–0.2 nA and at biases of 0.3–0.5 V. **a** Large scale 500×500 Å image. **b** 200×200 Å detail of the three nanotubes emerging from the lower right-hand corner of **a**. **c** Profile of the three tubes from the image **b**, along the direction marked and labeled with 1. **d** and **e** Other STM images of SWNT

HPLC and ^{13}C NMR analysis of the extracted and purified C_{60} sample.

It is interesting to note that the only fullerenes identified in the toluene extract of the nanotubes were C_{60} and, in very low proportion (5 times less than C_{60}), C_{70}. The formation of C_{70} on the catalyst surface can be explained as being the smallest elongated single-wall nanotube. In that case, only one layer of carbon (five C=C moieties) is added to the half C_{60} prior to its closure when extruded out of the catalyst particle.

2.2.6 Purification of the multi-wall carbon nanotubes. The HF treated samples – nanotubes free of zeolite – can be submitted to different oxidation [12, 26–29] and reduction [22] treatments to get rid of the amorphous carbon.

– Purification by permanganate oxidation: As a preliminary result of its oxidation, pure carbon nanotubes were obtained in 40% yield using the $KMnO_4/H_2SO_4$ aq. oxidation procedure reported by Ebbesen et al. [28]. On the TEM images of the corresponding product, it is possible to see lots of regular nanotubes of all shapes and with open tips. Moreover, no amorphous carbon was observed on these nanotubes.

Except for one single case, when we analyzed purified multi-wall nanotubes by STM, only tubes with diameters in the 10 nm range were found. On the single occasion, the two nanotubes with the estimated diameter in the 1-nm range were found partly embedded in amorphous carbon. The fact that these nanotubes were embedded in amorphous carbon material suggests that they were partially uncovered by the ultrasonication of the sample in toluene. The amorphous coating may be the reason why they survived to the oxidation treatment.

18

The surface area of the zeolite-free nanotubes – after HF treatment – was $653\,m^2g^{-1}$. For the further-purified sample by KMnO$_4$ oxidation – nanotubes free of zeolite and of amorphous carbon – the surface area was found to be $312\,m^2g^{-1}$. This lower value can be explained by the strong cohesion which reduces the outer surface of the material.

– Purification of the MWNT by air oxidation: 160 mg of pure nanotubes with open tips were obtained in 27% yield using dry air (12 ml/min) as oxidant for 3.5 h at 500 °C. The general aspect of the pure nanotubes can be seen in Fig. 4c.
– Purification of the MWNT by hydrogen reduction: The hydrogenation of the HF-treated samples was carried out at 900 °C (H$_2$/N$_2$: 10 /75 ml/min), for 4.5 h yielding pure nanotubes with open tips in 25%.

The three different purification procedures yielded long and short nanotubes in the same diameter range. A larger proportion of short nanotubes was observed in the purified products resulting from the cleavage of the nanotubes at the defects. The latter cleavages are more effective, giving a larger proportion of short nanotubes, by applying hydrogenation.

2.3 Applying clay support (preparation method B)

The layered crystalline clay used was originally a sodium silicate with a cation exchange capacity of 60 milliequivalent /100 g of clay material. The distance between the layers is a few nm depending on the cation.

Catalyst samples made by impregnation using clay have been tested in the decomposition of acetylene at 700 °C.
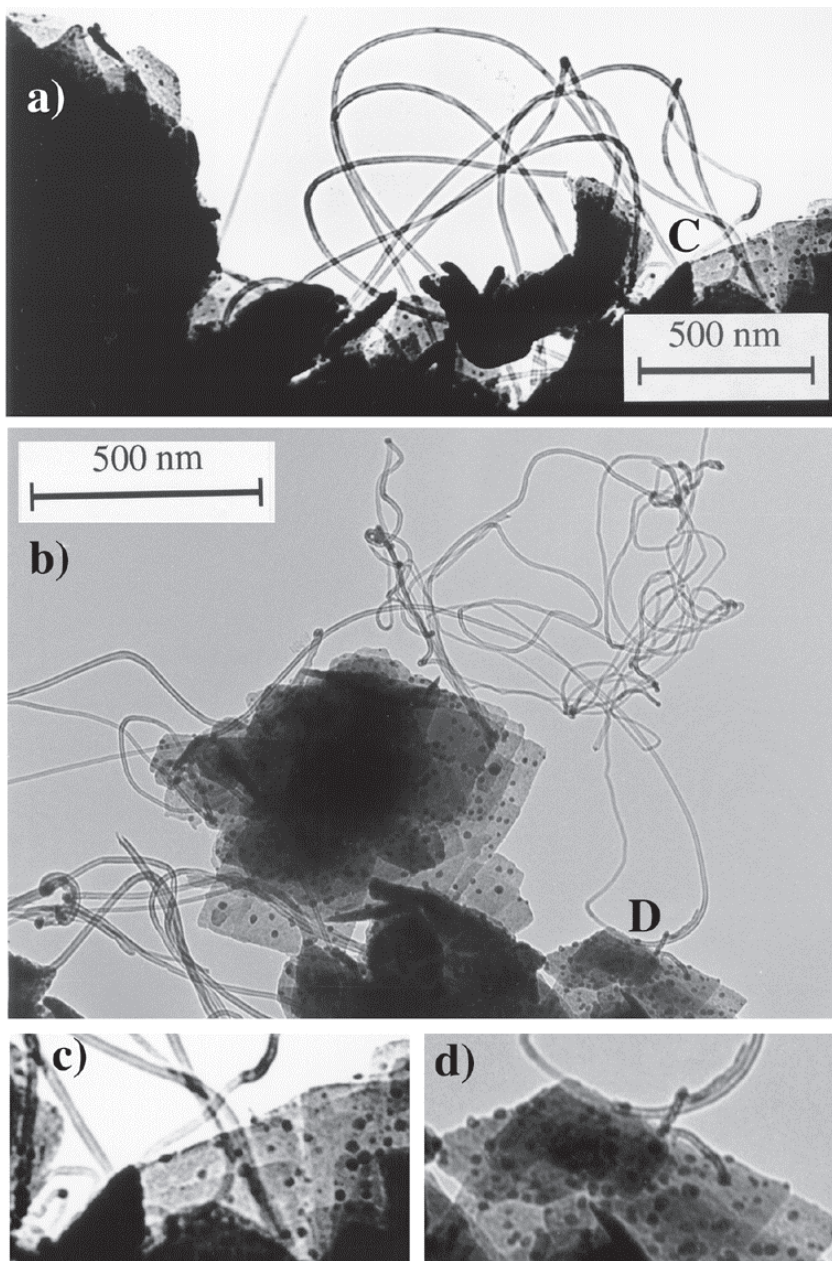
Fig. 6a–d. TEM images of carbon nanotubes formed in the catalytic decomposition of acetylene over metal/clay catalysts at 700 °C. **a** Fe/clay. **b** Co/clay. **c** 200% expansion of the region marked C in **a**. **d** 200% expansion of the region marked D in **b**

Co/clay and Fe/clay were found to have low activity in the formation of carbon nanotubes (12% and 10% carbon yield for a 30-min reaction, respectively). A view of the general aspect of the nanotubes formed over metal/clay is given in Fig. 6. In that figure, the grey-to-black part is the clay support and the black dots are the metal particles – active catalysts for nanotube-growing – formed under the reaction conditions. Only the metal particles on the outer surface of the clay samples are responsible for the nanotube-growing activity. The others, being in the interlayer, are inactive for steric hindrance reasons.

In Fig. 6c, the carbon nanotubes can be seen linked to the clay surface by their bottom ends through the metal particle. It is interesting to notice that no soot or mass of small nanotubes can be observed on the clay surface. Moreover, due to the transparency of some clay layers, it is possible to observe lots of particles in the interlayer of the clay support. As already observed for Co/silica catalysts [23], these catalyst particles have diameters in the same range as the inner diameter of the nanotubes formed on them [33].

2.4 General observations

As already mentioned, the global view of the different nanotube productions on the TEM images are rather similar. One way of getting more information on the small variations from one catalyst to another is by making the inner and outer diameter distribution histogram of nanotubes. Such an example is given in Fig. 7b for the Co/Silica 60-Å catalyst prepared at pH = 7.

The inner and outer diameters – distribution histograms – of nanotubes produced over the various Co-supported catalysts were measured and the results are reported in Table 3. In this table are also summarized the quality and quantity of the carbon deposit obtained after reaction. The catalysts were

prepared by method A at pH = 7 for silica and by method B for zeolite and for clay.

The results in Table 3 are explained according to a previous model [33] in the following. In that model, it was suggested that the diameters – inner and outer – are governed by the catalyst particle size and the flow rate of hydrocarbon at the catalyst particle surface. The nanotube length could be governed by the reaction time, whereas the nanotube turbostratic structure would depend on the reaction temperature.

2.4.1 Growth mechanism model for nanotubes on a catalyst particle during decomposition of hydrocarbons [33].

The growth of tubules during decomposition of acetylene can be explained in three steps – the decomposition of acetylene, the initiation reaction, and the propagation reaction. It is illustrated in Fig. 8 by the growing models of a perpendicular (5,5) and a parallel (9,0) tubule on identical catalyst particles.

The three important steps of the nanotube growth (Fig. 8) are these. First, dehydrogenative bonding of acetylene to the catalyst surface will free hydrogen and produce C_2 moieties bonded to the catalyst coordination sites. These C_2 units are assumed to be the building blocks for the nanotubes.

Second, at an initial stage, the first layer of C_2 units diffusing out of the catalyst remains at a Van der Waals distance from the C_2 layer coordinated to the catalyst surface. Then, if the C_2 units of that outer layer bind to one other, this will lead to a half fullerene. Depending on whether the central axis of that half fullerene is a threefold or a fivefold rotation axis, a (9n,0) or a (5n,5n) tubule will start growing respectively.

Third, the C_2 units are inserted between the catalyst coordination sites and the growing nanotube. The last C_2 units introduced will still be bonded to the catalyst coordination sites. From the catalyst surface, a new C_2 unit will again displace the previous one that becomes part of the growing tube, and so on.
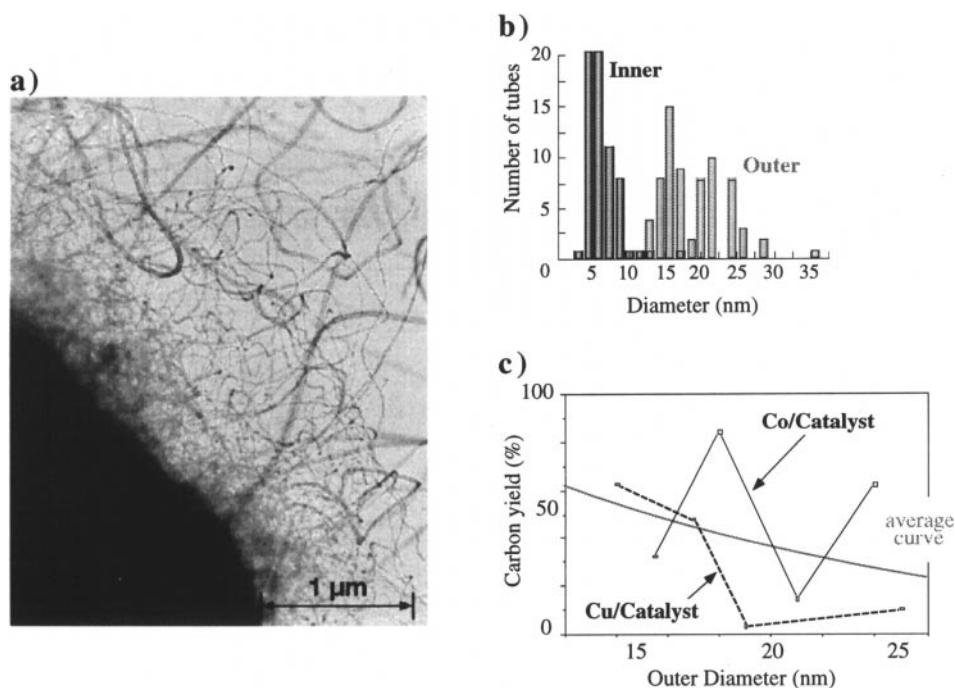

Fig. 7. a Carbon nanotubes formed in the decomposition of acetylene at 700 °C over a Co/Silica 60-Å catalyst (method A, pH = 7). **b** Diameter distribution histograms of nanotubes synthesized over a Co/Silica 60-Å catalyst. **c** Relation between the C_2H_2 conversion rate and the outer diameter of carbon nanotubes

Table 3. Inner and outer diameters of nanotubes produced over the various Co-supported catalysts

Support (Method)	Zeolite NaY 7.4 Å (B)	Clay (B)	Silica 20 Å (A)	Silica 40 Å (A)	Silica 60 Å (A)	Silica 90 Å (A)	Type of catalyst
MWNT	Long tubes. Regular diameters. Very few helices.	Few tubes. Regular diameters. Some helices.	Few tubes. Tubes covered by a thick layer of amorphous carbon.	Long tubes. Irregular diameters. Some helices. Tubes covered by a thin layer of amorphous carbon.	Long tubes. Regular diameters. Many helicoidal tubes.	Long tubes. Regular diameters. Thin layer of amorphous carbon on the tubes.	
Inner diameter nm[a]	2–9 (7)	2–12 (7)	(≈ 5)	4–9 (6)	3-17 (6) (6)	2–10 (4) 4–9 (5)	Ox. Red.
Outer diameter nm[a]	8–28 (15.5)	8–30 (15)	17–25 (21)	16–48 (24)	13–36 (18) (18)	8-28 (17) 11–29 (20)	Ox. Red.
SWNT	In bundles diameter = 1 nm	?	?	?	?	?	
(Global)[b] Carbon yield %	(++) 32	(+) 12	(-) 14	(++) 62	(+++) 71 76	(++) 50 50	Ox. Red.

[a] The diameters in brackets represent the average values.
[b] Best quality being turbostratic tubes with a small amount of amorphous carbon.
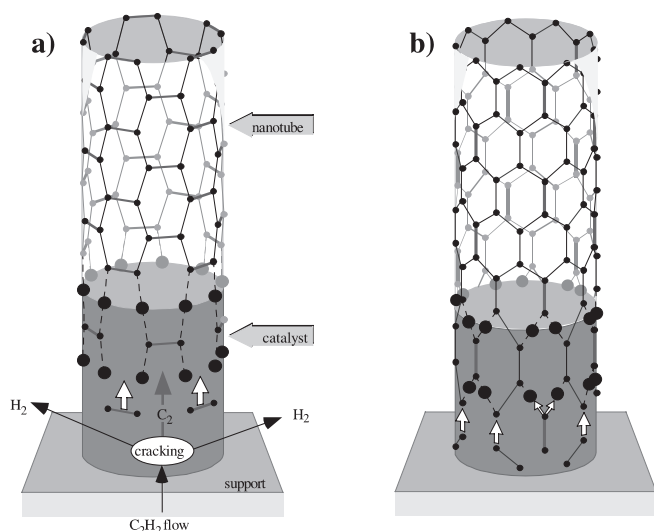
Fig. 8. a Schematic representation of a growing perpendicular (5,5) tubule on the corresponding catalyst particle. The catalyst contains many active sites but only those symbolized by black circles are directly involved in the (5,5) nanotube growth. The decomposition of acetylene is also represented on the same catalyst. **b** Growth of a parallel (9,0) tubule on a similar catalyst particle [33]

cles which migrate from the inner pores to the outer surface of the support, should have an optimum size of 60 Å for the tube growth. That optimum size of about 60 Å in diameter is maybe dependent on a stable carbon ring or cup that must form around the catalyst active particle prior to the nanotube growth. Otherwise, one would expect different preferential nanotube inner diameters according to the pore size of the supports (Table 3). Another optimum size of about 10 Å in diameter is also maybe stabilized over the metal/zeolite catalysts, producing fullerenes C_{60} and C_{70}, and single-wall nanotubes.

2.4.3 Control of nanotube outer diameter by the flow rate of hydrocarbon. According to Fig. 7c, the outer diameter of the nanotubes produced over Co/silica and Cu/silica catalysts seems to decrease when the C_2H_2 conversion rate (carbon yield) increases. When the activity is low – low carbon yield due to the presence of less-active sites – the C_2H_2 flow rate per active site is high and so the number of nanotube turbostratic layers is high, resulting in thicker nanotubes (Table 3).

2.4.4 Control of nanotube length by the reaction time. Catalytic behaviour of Fe/silica prepared by the ion-adsorption precipitation method was studied as a function of reaction time. In Table 4 carbon yield data are summarized. The amount of carbon deposit is increasing in time. After a reaction of 1 min, the macroscopic appearance of the sample

2.4.2 Control of nanotube inner diameter by the catalyst particle size. As seen from Table 3, the inner diameter of the nanotube formed seems to have a constant value of 6 nm whatever the pore size of the support. It is illustrated by the diameter distribution histogram represented in Fig. 7b, where the size distribution of the inner diameter is centred at around 6 nm. This value corresponds to the pore size of the silica 60 Å. Moreover, it is for the support silica 60 Å that we have obtained the best yields of carbon nanotubes (71%) with the best quality (+++), i.e. nanotubes not covered by amorphous carbon (Fig. 7a). These observations suggest that the pore size of the support and then, the size of the metallic parti-

Table 4. Carbon yield as a function of reaction time over Fe/silica (ion-adsorption precipitation at pH = 7) at 700 °C

Reaction time /min	1	5	10	30
Carbon yield /%	4.8	35.3	57.1	116.6

did not allow us to reach a conclusion on the presence of carbon nanotubes since it was not black but grey. Nevertheless, electron microscope observation verified the formation of nanotubes even after 1 min but only a few particles are covered by them. After 5 min all of the particles are overlaid by the nanotubes. It is interesting to note that significant deposition of amorphous carbon on the external surface of the nanotubes could not be observed even after a reaction of 30 min. At longer reaction times (> 1 h), deposition of soot begins on the outer surface of the tubes. It is also interesting to point out that there is no difference between the diameters of young (1 min) and old nanotubes (30 min). Only the length of the nanotubes is directly proportional to the reaction time and it is possible to interrupt the reaction and continue it later without affecting the quality of the produced nanotubes [23].

2.4.5 Control of nanotube turbostratic structure by the reaction temperature. Over the Co/support catalysts, it is possible to produce carbon nanotubes, of well-turbostratic structure, containing a very small amount of amorphous carbon by the decomposition of acetylene at 700 °C. Otherwise, decreasing or increasing the temperature by about 100 °C causes a decrease in the conversion rate of acetylene or an increase in the amount of amorphous carbon on the outer surface of the nanotubes, respectively. The nanotubes grown at low temperature (500 °C) are relatively free of amorphous carbon but the crystallinity of the turbostratic layers is poor. The deposition of amorphous carbon on the outer surface of the turbostratic nanotubes increases with the reaction temperature and with the reaction time. For a 5-h reaction using Co/silica the diameter of the amorphous carbon layer is up to ten times superior to that of the initial turbostratic nanotube. It is consistent with an autocatalytic mechanism of amorphous carbon formation, by hydrocarbon decomposition, over the turbostratic nanotubes wall. It is also in agreement with the previous results on nanotubes and amorphous carbon formation by hydrocarbon decomposition on graphite [23].

3 Conclusions

It is established that Co/silica catalysts which were prepared by ion-adsorption precipitation can produce carbon nanotubes of well-turbostratic structure with high activity and selectivity. The carbon deposition activity seems to be related to the cobalt content of the catalyst whereas the interesting nanotube formation selectivity seems to be a function of the pH of catalyst preparation. The calcination and/or hydrogenation steps of the catalyst preparation are not necessary and can even have an unfavourable effect on the catalyst performance. It is assumed that acetylene is able to reduce Co oxide under reaction conditions to the required extent, generating in situ the active sites for nanotube production.

With changing the pH of the original solution (between 7 and 9, method A), the quality of the carbon nanotubes, namely the amount of turbostratic straight and helical tubes, can be controlled to a certain extent.

Co/zeolite catalysts which were prepared by impregnation can also produce carbon nanotubes of well-turbostratic structure with high activity and even higher selectivity than Co/silica catalysts. Moreover, fullerenes and bundles of single-wall nanotubes were also found among the multi-wall nanotubes produced on Co/zeolite catalysts.

Purification of the multi-wall nanotubes was described in 0.25% and 25%–40% yields, relative to the deposited carbon, applying Co/silica and Co/zeolite catalysts, respectively.

The investigation of the effect of catalyst particle size and flow rate of hydrocarbon at the catalyst particle surface shed some light on the growth mechanism of carbon nanotube produced by the catalytic method previously proposed. As the diameter of the catalyst particle should be close to that of the inner tube, the number of turbostratic layers of each nanotube might depend on the flow rate of acetylene per active site. The turbostratic layers are assumed to be formed by C_2 units on the catalyst particle, exceeding those needed for the growth of the multi-shell nanotube inner layer. It behaves as if the nanotube length were governed by the reaction time, whereas the nanotube turbostratic structure depends on the reaction temperature.

References

1. H.W. Kroto, R.J. Heath, S. C O'Brien, R.F. Curl, R.E. Smalley: Nature **318**, 162 (1984)
2. S. Iijima: J. Phys. Chem. **91**, 3466 (1987)
3. S. Iijima: Nature **354**, 56 (1991)
4. H. Takaba, M. Katagiri, M. Kubo, R. Vetrivel, A. Miyamoto: Microporous Mater. **3**, 449 (1995)
5. K. Tanaka, K. Okahara, M. Okada, T. Yamabe: Fullerene Sci. Technol. **1**, 137 (1993)
6. E.G. Gal'pern, I.V. Stankevich, A.L. Chistykov, L.A. Chernozatonskii: Chem. Phys. Lett. **214**, 345 (1993)
7. N. Hamada, S. Sawada, A. Oshiyama: Phys. Rev. Lett. **68**, 1579 (1992)
8. P.M. Ajayan, S. Iijima: Nature **361**, 333 (1993)
9. D.H. Robertson, D.W. Brenner, J.W. Mintmire: Phys. Rev. B, **45**, 12529 (1992)
10. J.W. Mintmire, B.I. Dunlap, C.T. White: Phys. Rev. Lett. **68**, 631 (1992)
11. Y. Ando, S. Iijima: Jpn. J. Appl. Phys. **32**, 107 (1993)
12. T.W. Ebbesen, P.M. Ajayan: Nature **358**, 220 (1992)
13. S. Seraphin, D. Zhou, J. Jiao: Carbon **31**, 1212 (1993)
14. R.E. Smalley: In Proc. of The Robert A. Welch Foundation Conference on Chemical Research XXXVI "Regulation of Proteins by Ligands" (Houston, October 26-27 1992) p. 161
15. N. Hatta, K. Murata: Chem. Phys. Lett. **217**, 398 (1994)
16. S. Iijima, T. Ichihashi: Nature **363**, 603 (1993)
17. P.M. Ajayan, J.M. Lambert, P. Bernier, L. Barnedette, C. Colliex, J.M. Planeix: Chem. Phys. Lett. **215**, 509 (1993)
18. D.S. Bethune, C.H. Kiang, M.S. de Vries, G. Gorman, R. Savoy, J. Vazquez, R. Beyers: Nature **363**, 606 (1993)
19. S. Seraphin, D. Zhou, J. Jiao, J.C. Withers, R. Loutfy: Nature **362**, 503 (1993)
20. J.H. Hwang, W.K. Hsu, C-Y. Mou: Adv. Mater. **5**, 643 (1993)
21. A. Thess, R. Lee, P. Nikolaev, H. Dai, P. Petit, J. Robert, C. Xu, Y. Hee Lee, S. Gon Kim, D.T. Colbert, G. Scuseria, D. Tomanek, J.E. Fischer, R.E. Smalley: Science **273**, 483 (1996)

22. V. Ivanov, J. B.Nagy, P. Lambin, A.A. Lucas, X.B. Zhang, X.F. Zhang, D. Bernaerts, G. Van Tendeloo, S. Amelinckx, J. Van Landuyt: Chem. Phys. Lett. **223**, 329 (1994)
23. V. Ivanov, A. Fonseca, J. B.Nagy, A.A. Lucas, P. Lambin, D. Bernaerts, X.B. Zhang: Carbon **33**, 1727 (1995)
24. K. Hernadi, A. Fonseca, J. B.Nagy, D. Bernaerts, J. Riga, A.A. Lucas: Synth. Met. **77**, 31 (1996)
25. K. Hernadi, A. Fonseca, J. B.Nagy, D. Bernaerts, A. Fudala, A.A. Lucas: Zeolites **17**, 416 (1996)
26. T.W. Ebbesen, P. M Ajayan, H. Hiura, K. Tanigaki: Nature **367**, 519 (1994)
27. T.W. Ebbesen: Annu. Rev. Mater. Sci. **24**, 235 (1994)
28. H. Hiura, T.W. Ebbesen, K. Tanigaki: Adv. Mater. **7**, 275 (1995)
29. P.M. Ajayan, T.W. Ebbesen, T. Ichihashi, S. Iijima, K. Tanigaki, H. Hiura: Nature **362**, 522 (1993)
30. G.A. Somorjai, M.X. Yang: J. Mol. Cat. A: Chem. **115**, 389 (1997)
31. L.P. Biro, S. Lazarescu, Ph. Lambin, P.A. Thiry, A. Fonseca, J. B.Nagy, A.A. Lucas: Phys. Rev. B **56**, 12490 (1997)
32. L.P. Biro, J. B.Nagy, Ph Lambin, S. Lazarescu, A. Fonseca, P.A. Thiry, A.A. Lucas: Proc. 11th International Winterschool on Electronic Properties of Novel Materials, Molecular nanostructures, ed. by H. Kuzmany, J. Fink, M. Mehring, S. Roth (World Scientific 1997) p. 419
33. A. Fonseca, K. Hernadi, J. B.Nagy, Ph. Lambin, A.A. Lucas: Carbon **33**, 1759 (1995)